Martian Environmental Chamber: Dust System Injection

F. Cozzolino[1], V.Mennella[1], A.C.Ruggeri[1], G.Mongelluzzo[1,2],G.Franzese[1], C. I. Popa[1], C. Molfese[1],

F. Esposito[1], C.Porto[1], D.Scaccabarozzi[3].

Affiliations

[1] INAF – Osservatorio Astronomico di Capodimonte, Salita Moiariello 16, 80131 Napoli, Italy.

[2] Department of Industrial Engineering, University of Naples "Federico II", Piazzale Tecchio 80,

80125 Napoli, Italy

[3] Department of Mechanical Engineering Politecnico of Milano, via Gaetano Previati, 1/c, 23900 ,
Lecco, Italy

Abstract

The aim of this work is to describe the development and implementation of an experimental setup

able to reproduce some characteristics of the Martian atmosphere. The development of such setup fits

into the context of MicroMED project, that foresees the development of an optical particle counter to

be accommodated on the ExoMars 2020 Surface Platform, as part of the suite of sensors named Dust

Complex.

MicroMED will perform the first direct measurement of the size distribution of the powder close to

Martian surface. The experimental setup is able to reproduce the characteristics of the Martian

atmosphere: pressure, atmospheric composition, the actual temperature in which MicroMED will

operate (from -20 °C to 40 °C) and the most important thing: *the presence of suspended dust*.

The main result obtained in this work was to have found the right configuration of an experimental

setup in which to test sensors or instruments that work in Martian conditions. In particular, a dust

injection system has been developed in order to obtain a dust distribution without aggregations and

localized for a correct calibration of the instrument.

26

27

1. Introduction

Dust on Mars for years now has stirred the interest of the scientific community being it the protagonist of many phenomena observed on the planet, for example dust absorbs and scatters solar radiation, strongly modifying atmospheric thermal structure and balance. But the most spectacular events that are observed on Mars, where dust is the main actress, are local and global sandstorms and dust devils. The mechanisms of , transport and distribution of these phenomena are not yet well determined by the models (Kahre, 2006; Newman at al. 2002; Taylor, 2007) because, unfortunately, there is a lack of information on the physical characteristics of the grains such as size distribution and concentration. The only information available to date on physical characteristics of the powder has been provided by light absorbance measurements. Indeed, measuring the optical depth with complex calculations and making strong assumptions on the shape, on the refractive index of the particles, it is possible to obtain the effective radius of the airborn dust distribution.

Currently, there are different observations of the dust haze, performed using both the surface and orbital images (Toon et al., 1977; Drossart et al., 1991; Pollack et al., 1995; Tomasko et al, 1999; Greeley et al., 2006; Vasilyev et al., 2009; Fedorova et al., 2009; Vicente-Retortillo, et al., 2017). Currently, a direct study of the airborne dust has not been performed yet.

To provide a direct measurement of airborne dust, has been developed MicroMED (ScaccabarozziDiego et al 2018) , an optical particles counter capable of operating in Martian atmospheric conditions which was then selected for ExoMars 2020 Mission, onboard of the Surface Platform. MicroMED is an optical particle counter based on the light diffusion principle and is able to aspire the dust and analyze the light scattered from the single grains to measure their size and

51   abundance. It will operate directly close to the surface, where dust is lifted, allowing monitoring of

52   the dust injection into the atmosphere. MicroMED is part of the Dust Complex, a suite of five sensors

53   devoted to the study of Martian dust. Apart from MicroMED, the suite is composed by: Conductivity

54   Sensor, Impact Sensor, Electric Probes and EM-sensor in order to study the other events linked to the

55   lifted dust for example the electrical field. Indeed, airborne dust tends to acquire charge for

56   triboeletrification, the process depends on the grains composition and size (Kunkel, 1950; McCarty

57   and Whitesides, 2008; Melnik and Parrot, 1998; Desch and Cuzzi, 2000), as well on the

58   environmental conditions (Esposito et al., 2016, Harrison et al. 2016; Neakrase et al., 2016; Murphy

59   et al., 2016). Dust charging can lead to strong electric field, in theory able to overcome the Martian

60   electric breakdown (Farrell et al., 2017; Franzese et al., 2018).

61   In order to verify the performances and calibrate MicroMED, it was necessary to recreate the

62   atmospheric conditions that the instrument will find on Mars, in particular the presence of dusts.

63   The response of MicroMED to this condition has been simulated using a CFD (Computational Fluid

64   Dynamics) analysis in order to understand what are the critical parameters and the range of variation

65   that have to be guaranteed in laboratory (Mongelluzzo et al. 2018). In order to reproduce the Martian

66   conditions, a simulator chamber has been developed in which it is possible to recreate the Mars

67   atmospheric composition, pressure, temperature and dust concentration that MicroMED will face

68   during its operative time. Obviously, this type of setup can be used for the calibration of different

69   instruments such as impact sensors, microbalances and optical particle counters.

70   **2. Mars Atmosphere Simulator**

71   To recreate the atmospheric conditions of Mars in which is possible to verify the performances of

72   MicroMED, a cylindrical vacuum chamber has been used, called simulation chamber, as shown in

73   Figure 1 Vacuum chamber to simulate the Martian atmosphere.

74

75

76 **Figure 1** Vacuum chamber to simulate the Martian atmosphere

77 The average pressure on Mars is around 7 - 8 mbar (Zurek et al. 1992; Martinez G.M, et al. 2017).

78 This value was obtained in the simulation chamber, using a pumping system consisting of two cascade

79 pumps: a Varian Tri_Scroll 600 Series Dry Scroll and a Turbo V-750 Twis Torr. The pumping system

80 can generate a maximum vacuum of about 10^{-4} mbar in the chamber, therefore suitable for

81 reproducing the Martian pressure regime. The Scroll pump is also equipped with a VPI valve that

82 blocks the flow in the direction of the pump when it stops functioning. Pressure monitoring is

83 performed through the Pfeiffer compact capacitance gauge with a measurement range of 0-1000

84 mbar. The sensor is connected to an external controller that displays the value of the pressure in the

85 chamber.

86 In prevision of a MicroMED testing campaign, the chamber had to allow the injection of dust grains

87 of different sizes. In particular, in order to test the response of the instrument to calibrated

88 monodispersed grains, these have to remain separated from others. . Indeed, the electrification of the

89 grains could lead to the formation of aggregates, that in turn alter the size distribution in input

90 introducing a further level of uncertain.

91　An injection system has been realized capable of injecting a flow of thousands of separated grains

92　inside the chamber. The injection system had been developed and improved through several

93　intermediate steps, before obtaining the desired performance.

94　**3. Dry Injection System**

95　The first injection system, named Dry Injection, was made up of a holder containing the dry particles,

96　connected to the chamber through a gate valve. When the valve is opened, due to the pressure

97　difference between the holder (ambient pressure) and the chamber (1 mbar), the particles are aspired

98　into the chamber.

99　This injection system shows two problems:

100　1) *The flux of particles is focused in a very restricted area inside the chamber, so it is not uniformly*

101　*distributed.*

102　2) *The formation of groups of aggregated particles that represents a critical issue for the calibration*

103　*of the MicroMED optical particle counter.*

104　In order to verify the reliability of the system, several tests have been performed. To monitor the

105　distribution of grains inside the chamber, several aluminum stubs have been deployed on its base as

106　shown in Figure 2. Each stub was covered with an adhesive carbon disc on which the injected particles

107　could sediment. All carbon discs were then analyzed with a Scanning Electronic Microscope (SEM).
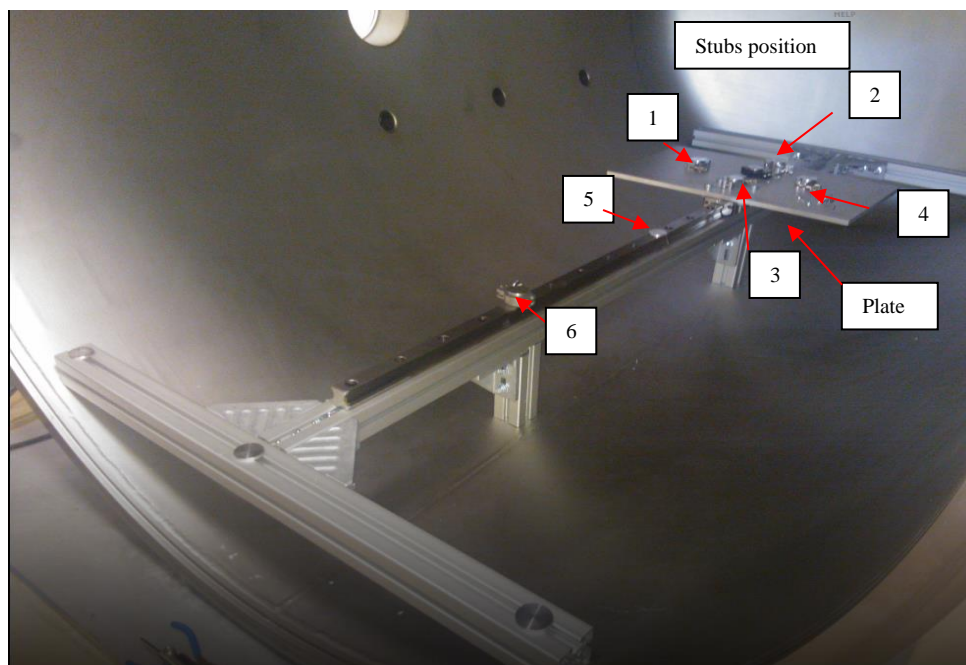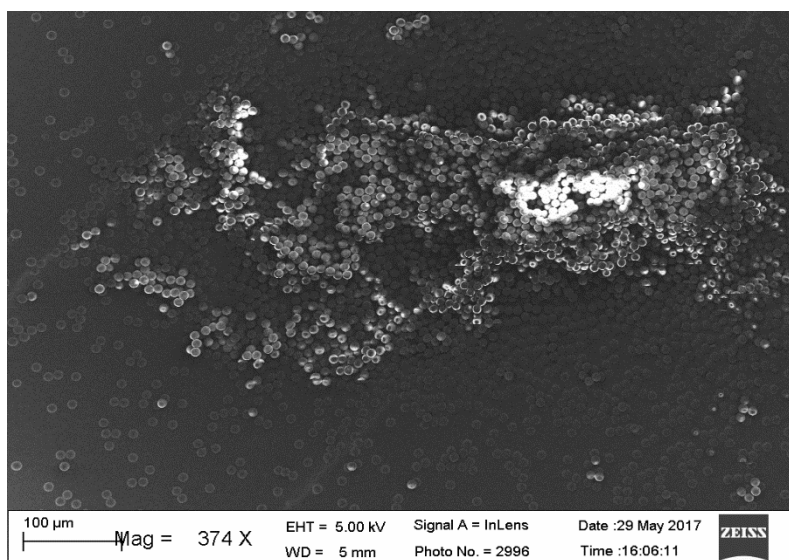
Figure 2 Aluminum Stub with Carbon Disc inside the simulation chamber in order to verify the particles distribution

.

108

109   Some samples, observed at the SEM, are shown in Figure 3 (single aggregate) and **Figure 4**(multiple

110   aggregates) . It is evident the formation of particles aggregates using a dry injection system .

111

112   **Figure 3** Local concentration of particles injected with dry system as observed over carbon stubs at the SEM.
113   Details of SEM. Parameters : Mag = Magnification, WD = Work Distance, EHT = Power Supply of Gun,
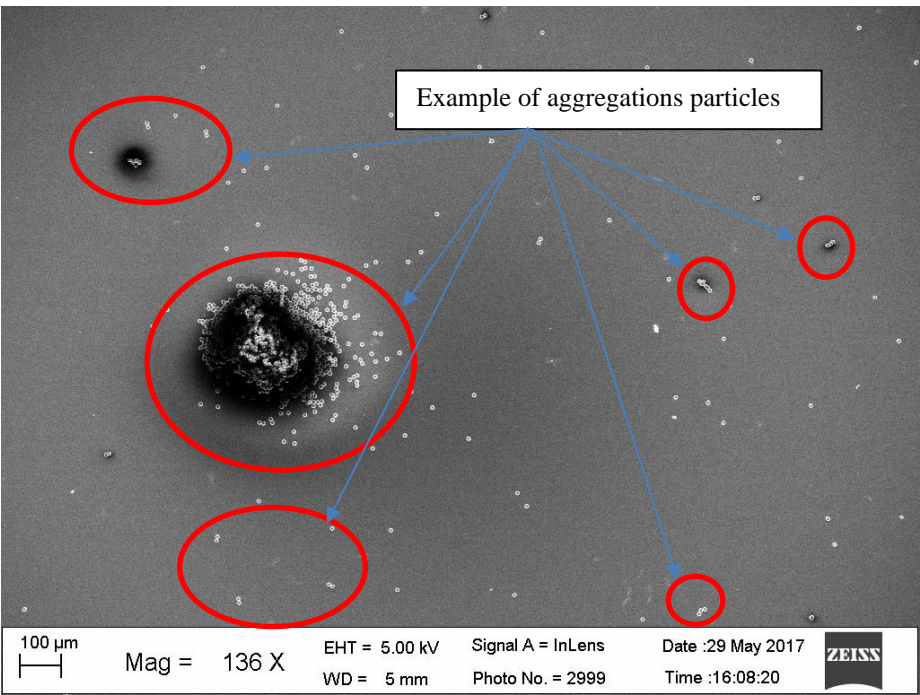114   Scale Bar = 100 µm

115

Figure 4 Several **e**vidence of particles aggregation in the chamber after injection of dry particles. Details of SEM. Parameters : Mag = Magnification, WD = Work Distance, EHT = Power Supply of Gun, Scale Bar = 100 µm

116

4. "Wet" Injection System

In order to solve the problem of the particle aggregates presented in the Dry Injection System, a

different injection system has been developed, using grains embedded in a solution.

The system shown in Figure 5 is constituted by a dispenser (Grimm Aerosol Dispensers mod 7811),

a second vacuum cylindrical chamber (pre-chamber), considerably smaller than the Martian vacuum

chamber, and a gate valve.

The used aerosol generator, is shown in Figure 6. It nebulizes a solution consisting of water and

particles to be injected into the pre-chamber. The nebulization is the reduction of a liquid in very

125 small parts (drops), which is obtained, for example, by colliding the liquid with a jet of air at high

126 speed, or forcing the liquid to pass through a very narrow orifice.

127 The solution before to be nebulized is placed in an ultrasonic chamber in order to well separate the

128 embedded grains.

129 Nebulizer flow rate is adjustable. The maximum flow rate is 7 l /min and is reachable at 1 atm

130 pressure. For our tests we set the flow rate at 7 l/min. The features of dispenser are summarized in

131 Table 1.

132

Supply Voltage	240 V	Aerosol Substance	Aqueous solutions
Frequency	50 to 60 Hz	Nebulizer flow rate	2.5 to 7.0 [l/min]
Maximum current	1.7 A	Dryer flow rate	7.5 to 17 [l/min]
Temperature Range	0 [°C] to 40 [°C]	Nebulizer liquid capacity	3 to 10 [ml]
Aerosol output air pressure range	Equal to atmospheric pressure	Particle concentration	$\geq 10^7 \, [1/cm^3]$

Table 1 Features of Grimm mod 7.811 Particle-Generator

133   The pre-chamber, has dimensions of 30 cm in diameter x 25 cm in height. The injection system is

134   connected to the top of the first chamber. Between the second and the first chamber there is the gate

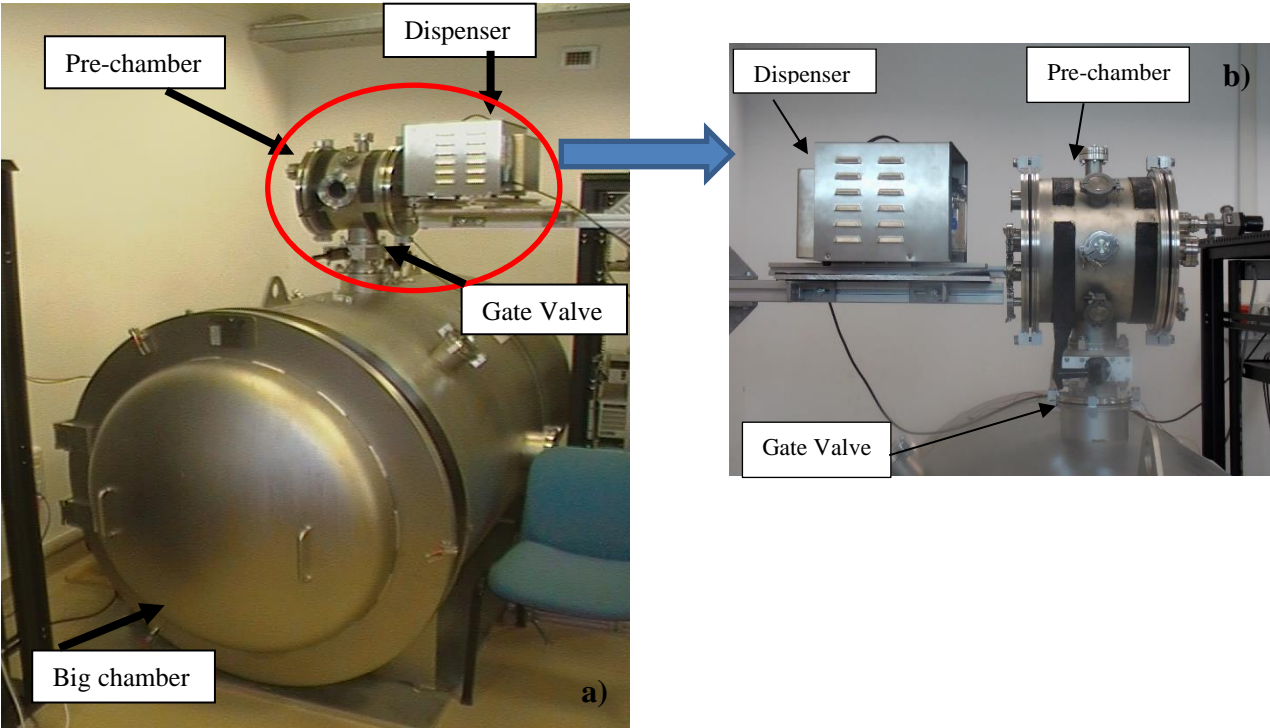135   valve as shown in Figure 5. The gate valve is operated by hand.

136

Figure 5 Martian Simulation chamber. **a)** The complete system; **b)** "Wet" injection system.

137   .
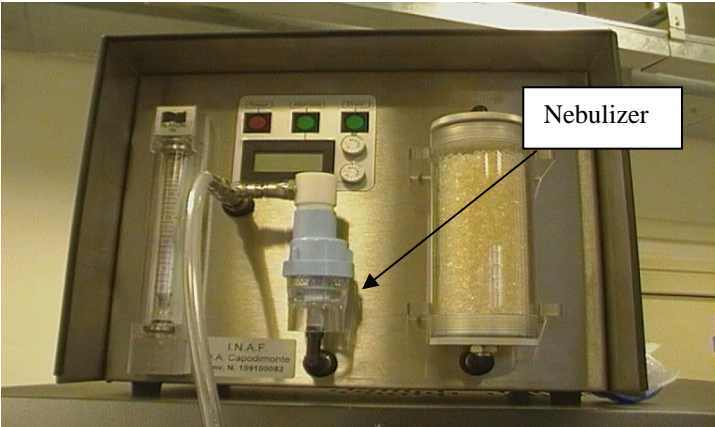
138

139

Figure 6 Particle Generator Model 7.811

140

141

4.1 Vacuum Pre-chamber

143 The   vacuum   pre-chamber   (Figure   7)   is   a   steel   cylinder   and

144 it has 4 flanges, 3 DN 40 and DN 15 1 on upper base,; on its side there are 4 flanges DN 40 and 2

145 DN 100 . On the lower base there are 3 flanges DN 40 and 1 DN 15 flange. All flanges are Iso K. The

146 flanges which will be used are: 1 DN 15 on the upper base of which will be connected to the output

147 of the aerosol generator, 1 DN 100 where the valve will be connected manual gate and a flange

148 reducing DN100-DN 15 on which connect the pipe coming from the large chamber (Martian

149 Simulation Chamber). The rest of the flanges will be closed with blind flanges.

150 The pressure in the pre-chamber will be 1 atm as required by the characteristics of the particle
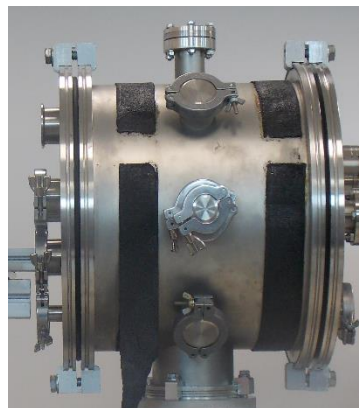
151 generator.

Figure 7 Vacuum Pre-Chamber

4.2 Big Vacuum Chamber (Martian Simulation Chamber)

162 The big vacuum chamber, where MicroMED will be tested, is a steel cylinder with 1,34 m in diameter

163 and 2,05 m in length. It is provided on the upper part of a window DN 160 and three flanges DN 15

164 to one of which will be connected to the pipe coming from the pre-chamber. At theside there are 2

165 windows DN 160, 3 flanges DN 60, one of which will be used to feedthrough liquids for a future

166 cooling system, 2 flanges DN 100 to one of which will be connected with a flange feedthrough that

167   will allow us to power with 6 V the MicroMED pump from the outside. The internal pressure will be

168   increased to 6 mbar using a scroll pump Agilent mod TS600 220V 1 Ph. The chamber is provided of

169   an internal moving aluminum panel that can slide on a track system in order to set its position. During

170   the phase of testing, MicroMED will be placed on this base. The vacuum chamber is connected to

171   the vacuum pre-chamber by a steel tube, which will guide the passage of the particles in the main

172   chamber.

173   **5. Measurements of particle distribution in Martian simulation chamber**

174   Once the Simulator Chamber was implemented, a series of measurements were carried out to verify

175   the functionality of the injection system and the distribution of the particles in the simulation chamber.

176   Aluminum stubs have been positioned same as above mentioned (Figure 2). The injection system

177   generates an aerosol of particles that is distributed inside the pre-chamber.

178   When the gate is opened, due to the difference in pressure between the simulation chamber (1 mbar)

179   and pre-chamber (1 atm) the particles are sucked with high speed into the simulation chamber. The

180   particles bounce on the bottom of the chamber and are spread. Once the equilibrium condition of 6

181   mbar is reached, the bounced particles deposit for gravity on the discs positioned at the base of the

182   chamber. At the end of the settling process the discs are analyzed with the SEM.

183   The disks have been numbered, each corresponding to a precise position within the chamber. At the

184   end   of   the   settling   process   the   disks   are   analyzed   with   the   SEM.

185   The disks have been numbered, each corresponding to a precise position within the chamber. In

186   particular, the disks 3, 4, and 5 have been positioned at the gate valve which represents the entry of

187   the particles in the simulation chamber. The disks 1, 2 and 6 have been positioned respectively at one

188   meter from the disk 3, at 0.7 meters from disk 3 and 0.15 cm from disk 5.

189

190   The test was performed using monodispersed particles with size 0.5, 1.30, 2.8, 4.32, 6.36, 8.43, 11,

191   14.98 μm. The same set of particles has been used during the calibration of MicroMED. From the

192   analysis of the stubs to the SEM it is evident that injecting the particles with this injection system
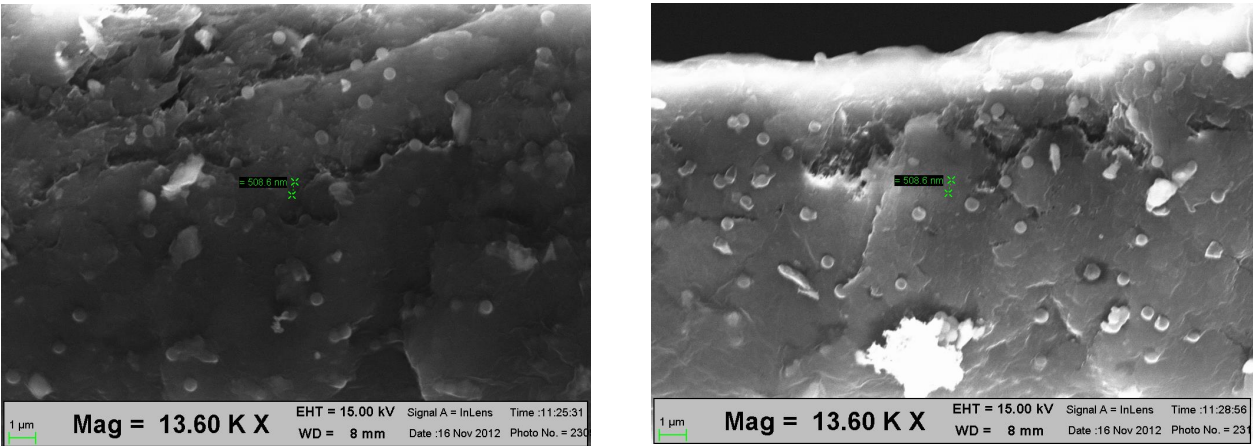

Figure 8 Absence of aggregates particels injected with the Wet Injection System disk 3 (on the right) and disk 5 (on the left). The green marker shows the size of particles, it is 508.6 nm

193   avoids the formation of the aggregates of particles how shown in Figure 8that were present with the

194   dry injection system.

195   The results about distribution particles inside the big chamber are shown in Figure 9, where is shown

196   the trend of the numerical density of the particles as a function of the position of the disks, for each

197   used particle size.
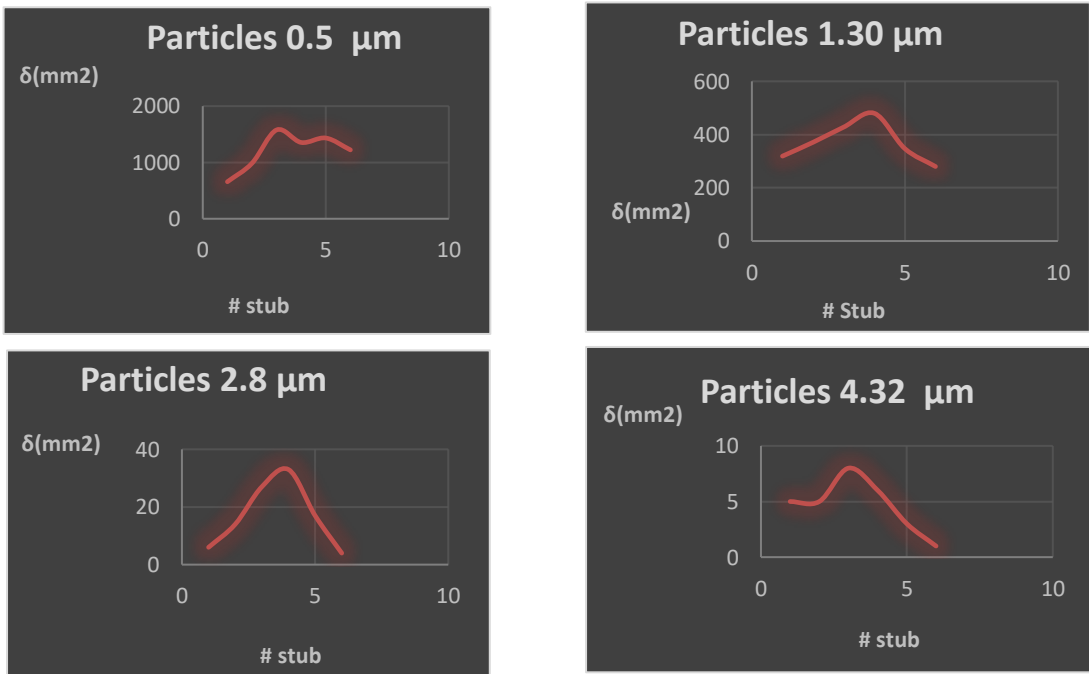
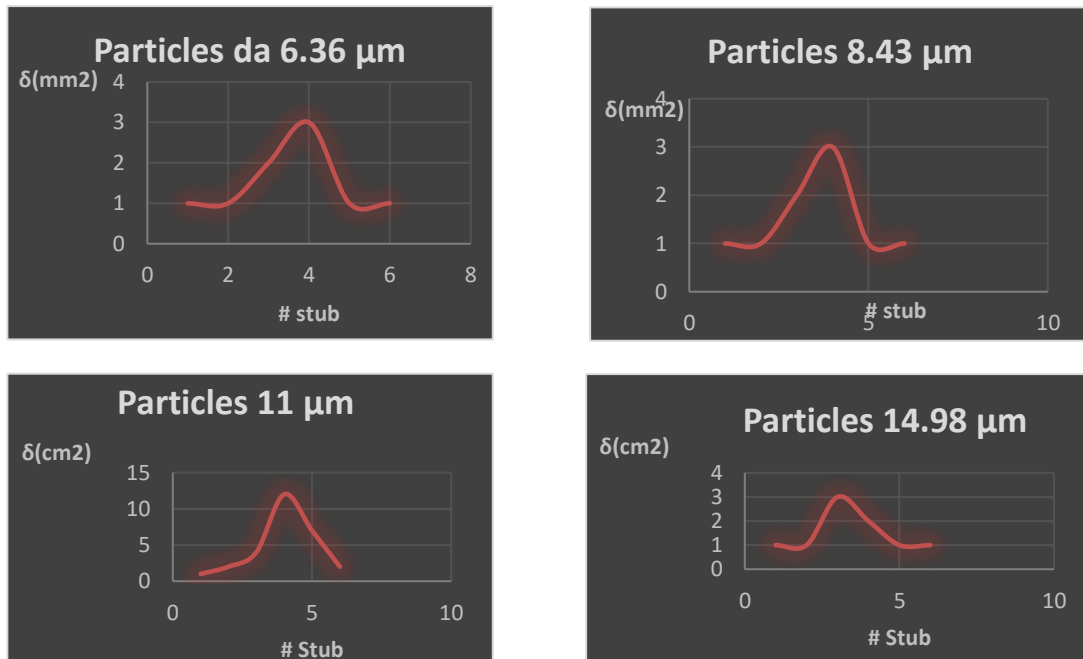**Figure 9** Particle distribution according to the position of the sampling discs positioned in the simulation chamber. Y-axis shows the density value, while x-axis the position of the disks

.

The plots show that the "wet" injection is able well spread into the simulation chamber the dust grains on the whole size range considered. The smaller particles tend to disperse more, distributing almost uniformly throughout the chamber, while the larger diameter particles tend to be distributed in the region corresponding to their entrance area (the area under the gate valve).
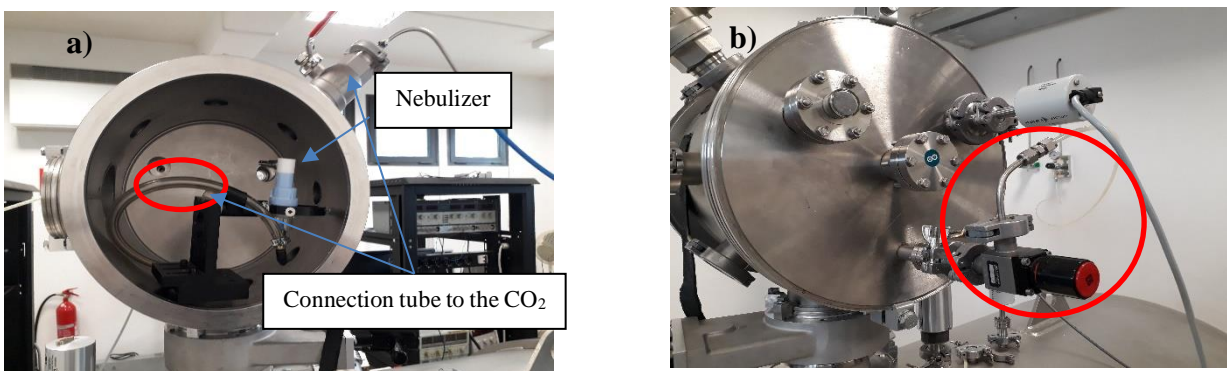

Figure 10 a) Nebulizer inside the pre-chamber connected to system injected of CO_2 **b)** System injected of CO_2

The injection system that makes use of the dispenser has a limitation, because it only works in presence of 1 bar atmosphere, so it can inject particles into the pre-chamber only if it has a pressure

227   of 1 bar. The consequence of this is that when the gate valve between the pre-chamber and the

228   simulation chamber is opened, a strong pressure difference causes the particles to acquire a very high

229   speed, so to bounce on the chamber bases and wall before being sampled by MicroMED. This causes

230   a large dispersion and loss of particles. To improve this aspect, it has been simplified the particle

231   injection system to control the input velocity of the particles in the simulation chamber. As shown in

232   Figure 10, the Grimm dispenser was removed and just the nebulizer was placed, filled up with a

233   solution of ethanol and particles, inside the pre-chamber connecting it to the CO_2 (Figure 10) injection

234   system of the chamber. This configuration allows to inject the particles after having depressurized

235   the pre-chamber (for example, bringing it to 15 - 16 mbar) with a pump, in order to control the

236   pressure gap between the two chambers, as well as the particle velocity.

237   We used the ethanol instead of water for the particles solution in order avoid the freezing during the

238   rapid gas expansion experienced caused by the gate opening. Ethanol is a very volatile liquid which

239   evaporates at a pressure of 6 mbar and with a temperature of about 22°C, depositing on the walls of

240   the chamber. Several measurements were made by injecting only ethanol to understand if the droplets

241   that are generated could somehow be sucked. Test results show that MicroMED does not reveal

242   ethanol.

243

244

245   *6 MicroMED BreadBoard performance test*

246   Using the results presented in the last section, it was possible to identify the optimal position where

247   the grains concentration peaks. In this position, corresponding to the disks 3 and 4, we installed a

248   BreadBoard version of MicroMED, as shown in Figure 11, in order to perform the first tests of the
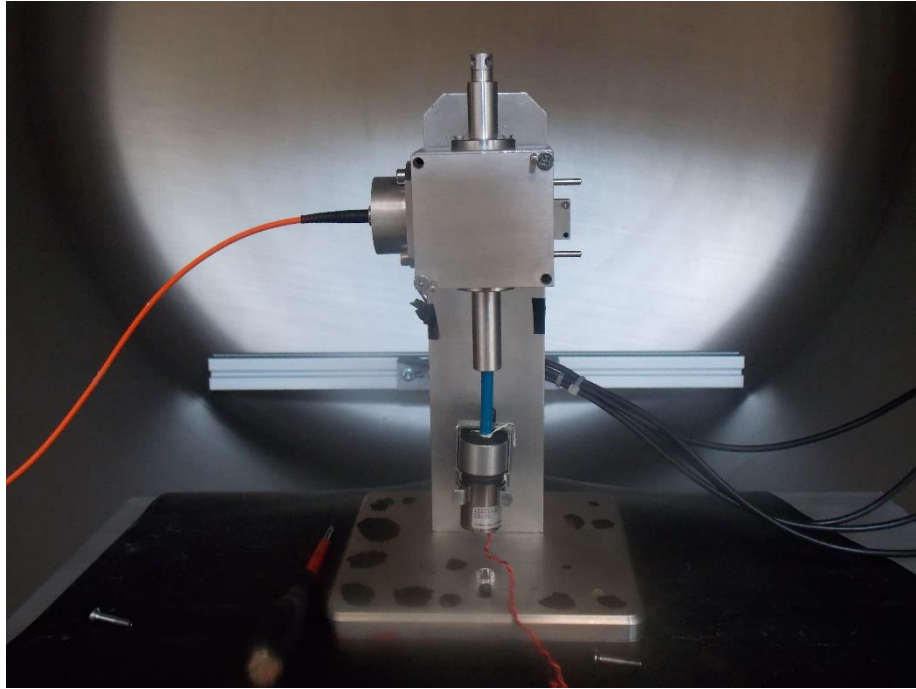
249   sensor performances.

250

251   **Figure 11** BreadBoard version of MicroMED installed in the simulation chamber

252

253   The tests performed with the upgraded injection system showed an increase in the number of particles

254   acquired by MicroMED.

255   Table 2 shows the average amplitude values of the signals generated by the particles sucked by

256   MicroMED, for grain size of 0.448, 1.046, 4.051, 8.496 micrometers. The particle signals were

257   acquired using an electronic board having two channels with different amplification stage called Low

258   and High. The Low channel was used for the study of the signals of the particles with a diameter

259   greater than 2 microns and had an amplification factor of 10^5, while the High channel was used for

260   the study of the signals of the particles with a diameter less than 2 microns and had the amplification

261   factor of 10^7.

262   An example of the signals acquired by MicroMED BreadBoard in both channels are shown in Figure

263   12
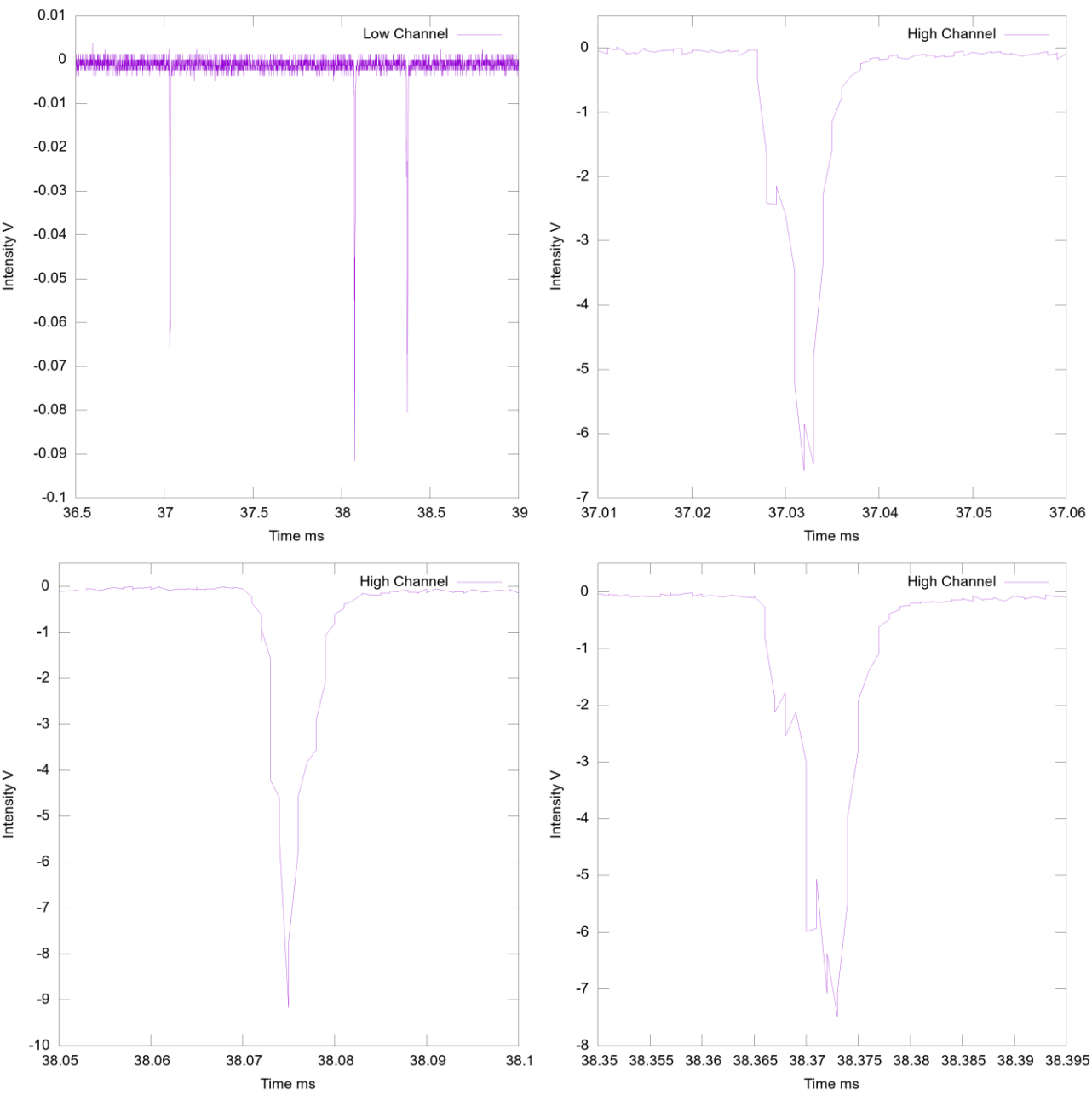
264

265   **Figure 12** Example of the signals acquired by MicroMED BreadBoard. The first plot on top left shows an extract of the
266   time series acquired in Low channel during the particles injection: three passing grains are visible. The successive plots
267   show a zoom of these three signals in High channel.

268

Channel	Size (μm)	Number Signals	Mean (V)	Median (V)	Standard Deviation (V)	Lower Quartile (V)	Upper Quartile (V)
High	0.448	150	0.18	0.17	0.09	0.11	0.25
High	1.046	113	2.4	1.9	1.7	1.2	3.4

Low	4.051	135	0.18	0.15	0.19	0.09	0.20
Low	8.496	145	0.47	0.29	0.49	0.18	0.52

269   **Table 2** The results in volt of the MicroMED BreadBoard acquisitions for the test with monodispersed spherical grains.

270   .

271

272   In Figure 13 two amplitude distribution of signals for High and Low channels are shown.

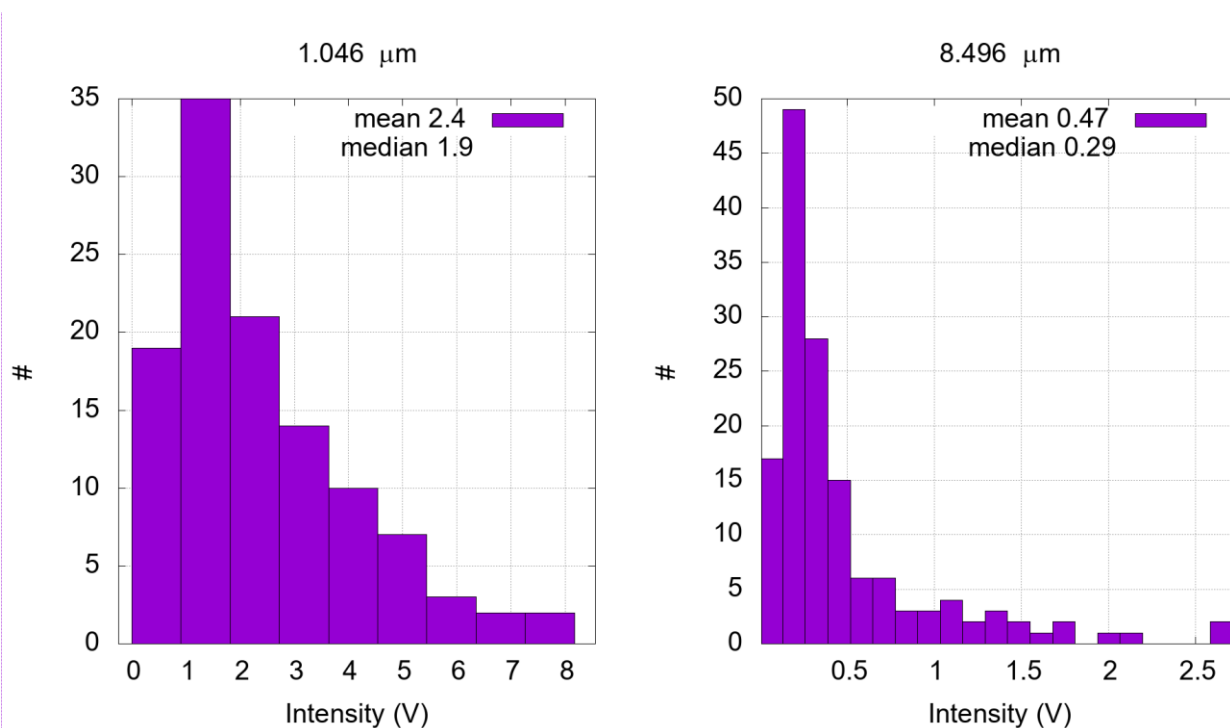274   **Figure   13**   Intensity   distribution   of   the   signals   acquired   in   by   MicroMED   BreadBoard:
275   left) High Channel for the injection of a monodispersed samples of 1.046 micron spherical grains;
276   right) Low Channel for the injection of a monodispersed samples of 8.496 micron spherical grains.

277   The average values of the amplitudes, shown in Table 2, were compared with the theoretical

278   instrumental response of MicroMED, obtained from the Mie model. A good agreement between the

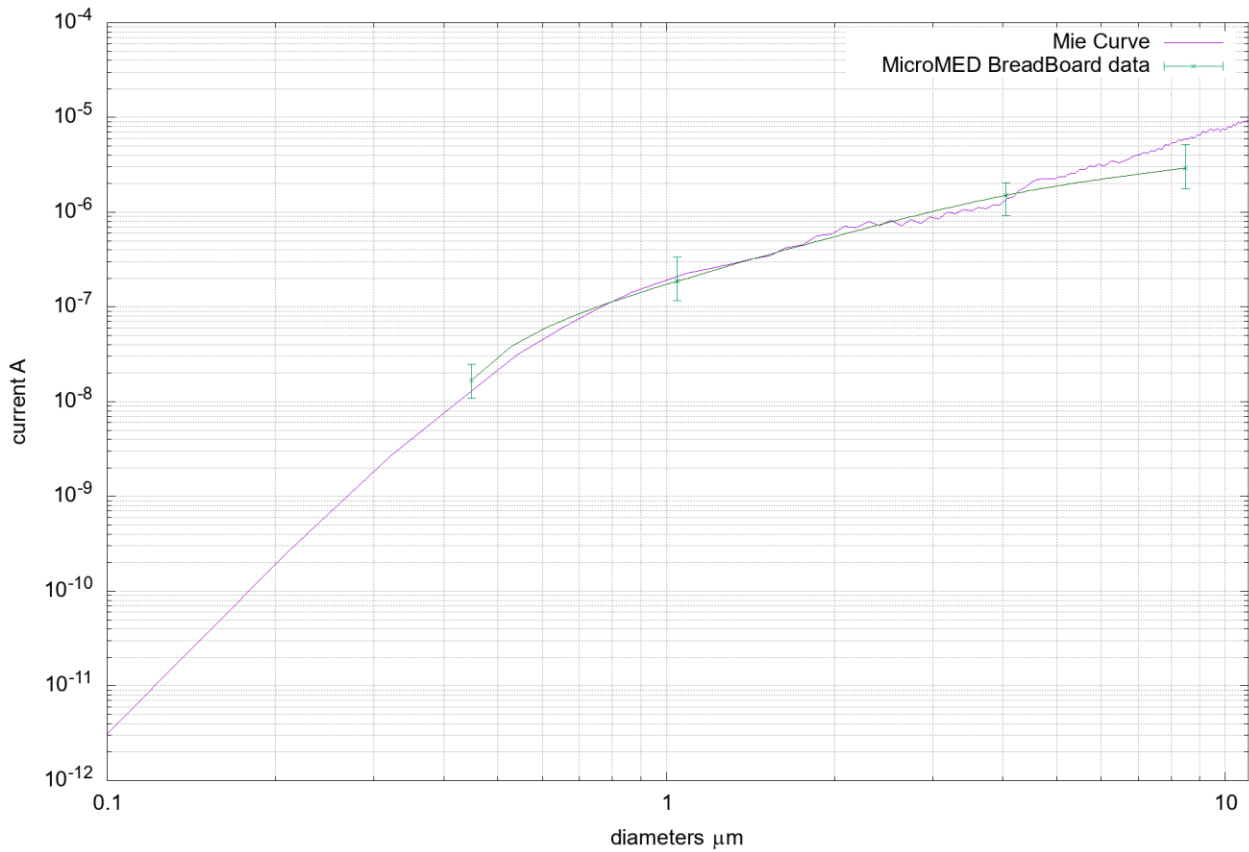279   theoretical and experimental trend can be seen in Figure 14.

280

Figure 14 Comparison of the signals current obtained from the MicroMED BreadBoard measurements and the average theoretical Mie curve expected.

7 . Conclusions

The next ESA/Roscosmos ExoMARS 2020 missions aim to investigate possible life traces on the Martian surface and study the Martian past and present climate, in order to address its sustainability for the life. To achieve this goal, it is fundamental to perform a proper characterization of the atmospheric dust and its interactions with the Martian weather.

MicroMED is an optical particle counter on board of the surface lander, as part of the Dust Complex, a suite of instruments aimed to the study of the characteristics of the primary lifted dust. In particular, MicroMED will acquire the first direct measurement of the primary dust amount and size distribution.

In order to develop the instrument, we realized a Martian simulation chamber able to reproduce the environment where MicroMED will operate. Here, the most important goal reached has been the

294   development of the correct configuration of the injection dust system, in order to obtain a dust

295   distribution without aggregations and localized near the instrument.

296   The Dust Injection System is constituted by a system of vacuum chambers that allows the injection

297   of dust particles in a controlled CO_2 low pressure environment. We decided to inject the dust grains

298   inside the chamber in an ethanol solution, in order to generate a flux of particles without aggregations.

299   With this new injection system the following improvements are reached:

300   1) possibility to vary the flow velocity by acting on the pressure difference between the pre-chamber

301   and the simulation chamber;

302   2) direct injection of CO_2 and particles to simulate the Martian atmosphere;

303   3) the avoid of particle losses.

304   Indeed, the ethanol acts as a protective membrane for particles preventing triboelectric effects that

305   cause aggregates.

306   The Martian simulation chamber is currently used during the development of the MicroMED for tests

307   and calibrations.

314 **References**

315   1. Scaccabarozzi, Diego, et al. "MicroMED, design of a particle analyzer for Mars",

316   *Measurement* 122 (2018): 466-472,

317   2. Bourke, M. C., K. S. Edgett, and B. A. Cantor (2008), Recent aeolian dune change on Mars,

318   *Geomorphology*, 94, 247–255, doi:10.1016/j.geomorph.2007.05.012.

319   3. Desch, S.J., Cuzzi, J.N., 2000. The generation of lightning in the solar nebula. Icarus143 (1),

320   87–105.

321   4. Drossart, P. et al., "Martian aerosol properties from the Phobos/ISM experiment", Annales

322   Geophysicae 9, 754-760, 1991.

323   5. Esposito, F., Molinaro, R., Popa, C. I., Molfese, C., Cozzolino, F., Marty, L., ... & Ori, G. G.

324   (2016). The role of the atmospheric electric field in the dust-lifting process. *Geophysical*

325   *Research Letters*, *43*(10), 5501-5508.

326   6. Farrell, W.M., McLain, J.L., Collier, M.R., Keller, J.W., 2017. The Martian dust devil

327   electron avalanche: laboratory measurements of the E-field fortifying effects of dust-electron

328   absorption. Icarus297, 90–96.

329   7. Fedorova, A. A. et al., "Solar infrared occultation observations by SPICAM experiment on

330   Mars-Express: Simultaneous measurements of the vertical distributions of $H2O$, $CO2$ and

331   aerosol" Icarus 200, 96-117, 2009. doi:10.1016/j.icarus.2008.11.006

332   8. Franzese, G., Esposito, F., Lorenz, R., Silvestro, S., Popa, C. I., Molinaro, R., ... & Deniskina,

333   N. (2018). Electric properties of dust devils. *Earth and Planetary Science Letters*, *493*, 71-

334   81.

335   9. Martínez, G.M., Newman, C.N., De Vicente-Retortillo, A., Fischer, E., Renno, N.O.,
336   Richardson, M.I., Fairén, A.G., Genzer, M., Guzewich, S.D., Haberle, R.M. and Harri,
337   A.M., 2017. The modern near-surface Martian climate: A review of in-situ meteorological
338   data from Viking to Curiosity. Space Science Reviews, 212(1-2), pp.295-338.

340   10. Vicente-Retortillo, Á., G. M. Martínez, N. O. Renno, M. T. Lemmon, and M. de la Torre-
341   Juárez (2017), Determination of dust aerosol particle size at Gale Crater using REMS UVS
342   and Mastcam measurements, Geophys. Res. Lett., 44, doi:10.1002/2017GL072589.

345   11. Kunkel, W.B., 1950. The static electrification of dust particles on dispersion into a cloud. J.

346   Appl. Phys.21 (8), 820–832.

347   12. McCarty, L.S., Whitesides, G.M., 2008. Electrostatic charging due to separation of ions at

348   interfaces: contact electrification of ionic electrets. Angew. Chem., Int. Ed. Engl.47 (12),

349   2188–2207.

350   13. Melnik, O., Parrot, M., 1998. Electrostatic discharge in Martian dust storms. J. Geo-phys.

351   Res. Space Phys.103 (A12), 29107–29117.

352   14. Mongelluzzo, G., Esposito, F., Cozzolino, F., Molfese, C., Silvestro, S., Popa, C. I., ... &

353   Scaccabarozzi, D. (2018, June). Optimization of the fluid dynamic design of the Dust Suite-

354   MicroMED sensor for the ExoMars 2020 mission. In 2018 5th IEEE international workshop

355   on metrology for aerospace (MetroAeroSpace) (pp. 134-139). IEEE.

356   15. Pollack, J. B. et al., "Viking Lander image analysis of Martian atmospheric dust" Journal of

357   Geophysical Research 100, 5235-5250, 1995. doi:10.1029/94JE02640

358   16. Silvestro, S., Fenton, L. K., Vaz, D. A., Bridges, N. T., & Ori, G. G. (2010). Ripple migration

359   and dune activity on Mars: Evidence for dynamic wind processes. *Geophysical Research*

360   *Letters*, *37*(20).

361   17. Silvestro, S., Vaz, D. A., Di Achille, G., Popa, I. C., & Esposito, F. (2015). Evidence for

362   different episodes of aeolian construction and a new type of wind streak in the 2016 ExoMars

363   landing ellipse in Meridiani Planum, Mars. *Journal of Geophysical Research: Planets*,

364   *120*(4), 760-774.

365   18. Tomasko, M. G. et al., "Properties of dust in the Martian atmosphere from the Imager on

366   Mars Pathfinder" Journal of Geophysical Research 104, 8987-9008, 1999.

367   doi:10.1029/1998JE900016.

368   19. Toon, O. B. et al., "Physical properties of the particles composing the Martian dust storm of

369   1971-1972", Icarus 30, 663-696, 1977. doi:10.1016/0019-1035(77)90088-4.

370   20. Vasilyev, A. V.; Mayorov, B. S.; Bibring, J.-P., "The retrieval of altitude profiles of the

371   Martian aerosol microphysical characteristics from the limb measurements of the Mars

372   Express OMEGA spectrometer", Solar System Research, Volume 43, Issue 5, pp.392-404,

373   2009.

374   21. Zurek, R. W., Barnes, J. R., Haberle, R. M., Pollack, J. B., Tillman, J. E., & Leovy, C. B.

375   (1992). Dynamics of the atmosphere of Mars. *Mars*, 835-933.

376   22. Harrison et al.2016. *Applications of Electrified Dust and Dust Devil Electrodynamics to*

377   *Martian Atmospheric Electricity* Space Sci Rev (2016) 203:299–345.

378   23. Neakrase et Al.,2016. *Particle Lifting Processes in Dust Devils* Space Sci Rev (2016)

379   203:347–376.

380   24. Murphy et Al.,2016. *Field Measurements of Terrestrial and Martian Dust Devils*

381   Space Sci Rev (2016) 203:39–87.

382   25. Newman et Al 2002**.** Modeling the Martian dust cycle, 1. *Representations of dust transport*

383   *processes* JOURNAL OF GEOPHYSICAL RESEARCH, VOL. 107, NO. E12, 5123**.**

384   26. Kahre et Al 2006. *Modeling the Martian dust cycle and surface dustreservoirs with the NASA*

385 *Ames general circulationmodel* JOURNAL OF GEOPHYSICAL RESEARCH, VOL. 111, E06008.

386   27. Taylor et Al. 2007. *Modelling dust distributions in the atmospheric boundary layer on Mars.*

387 Boundary-Layer Meteorology volume 125, pages305–328(2007).

388

389

390

391

392

393

394
395